Journal of Engineering Mathematics **30:** 307–320, 1996.

Composite, Navier–Stokes and Euler unsteady-flow computations in boundary layers

FRANK T. SMITH
Department of Mathematics, University College London, Gower Street, London WC1E 6BT, U.K.

Received 18 October 1993; accepted in revised form 23 February 1995

Abstract. Computational approaches based on previous nonlinear theoretical findings are developed for a Composite system, the Navier–Stokes system, and the Euler system of equations, in turn, with applications to incompressible boundary-layer transition and dynamic stall. The emphasis is on schemes appropriate for medium-to-large Reynolds numbers, and so as a start the computations are kept to two spatial dimensions. The Composite scheme is developed first, including significant normal-pressure-gradient effects as suggested by the theory. The same scheme is then modified to accommodate, iteratively, the Navier-Stokes form and then the Euler form, for comparison. The agreement between the three sets of results tends to be very close in the parameter ranges studied. The necessary extensions of the work are also discussed.

1. Introduction

Computational studies of unsteady disturbed flow produced within a boundary layer are described in this article, the computations being based on Composite, Navier–Stokes- and Euler-equation representations. The potential applications to understanding and prediction of boundary-layer transition and to unsteady airfoil computations are uppermost in mind here, along with a number of other motivations and issues which are addressed subsequently. These include the questions of whether a time-marching computational approach can possibly be used as an engineering tool at large Reynolds numbers, e.g. for transition prediction, whether in particular a two-dimensional time-marching treatment is able to capture significant aspects of transition to turbulence (see also below), and whether the approach can provide any fresh insight into transition prediction and transition criteria. Continuing new insight, especially of a nonlinear kind as here, is certainly needed in this area of transition and especially for by-pass transition processes, which partly form the background for the present investigation; there is also much interest in, and connection with, the closely related areas of unsteady separation and dynamic stall. Again, it is well known that the global effects of unsteady boundary-layer displacement, receptivity, and most of all transition, are often considerable in unsteady airfoil oscillations.

Most aerodynamic interest is in the medium-to-high Reynolds number range, within the present contexts. For that reason a Composite scheme, suggested by asymptotic scaling theories to a great extent, is applied and tested first, rather than the more conventional Navier-Stokes DNS approaches which tend to be restricted to relatively low Reynolds numbers, from accuracy and/or cost considerations, or Euler approaches which miss the viscous production. This Composite scheme (which tackles a reduced set of equations, as in Smith *et al.* [1]) is then used subsequently as the springboard for an apparently novel NS approach also, as well as for an Euler-equation approach, given the advantages of such reduced-equation schemes demonstrated in steady aerodynamic computations. Again, there are areas of unsteady

aerodynamics, for example in unsteady separation and dynamic stall, where rather leaner devoted schemes, which improve with increasing Reynolds number instead of deteriorating, also seem to be needed. One might hope indeed to apply the present treatment or its like to cover the unsteady boundary-layer flow over an entire airfoil, as opposed to the current emphasis on local features; that hope may or may not be far-fetched. The more local treatment here however is intended eventually to provide extra data, or alternative data, on transition, to compare with the empirical transition rules (e.g. Van Driest and Blumer [2], Dunham [3], Roberts [4], Abu-Ghannam and Shaw [5], Narasimha [6], Van Ingen [7]) and to attempt to detect trends on for instance the influences of free-stream turbulence and airfoil-scale oscillations. Another aspect to note is that of comparing with recent asymptotic theoretical predictions, including the formation of a logarithmic wall layer and local bursting phenomena predicted by two-dimensional theory (Smith [8], Hoyle *et al.* [9], Smith *et al.* [10]) and the possibility of incorporating such more recent theory as further guidance for the numerical approach as here.

The computational approaches developed in the present work, for unsteady boundary layers, are suggested by recent theoretical findings ([8], [9] and [11]) and by the computational procedures developed in Smith *et al.* [1] mainly for channel flows. In this last work, good agreement between Composite and NS results was found on linear stability features over a wide range of Reynolds numbers, even as low as approximately 1/10 of the critical Reynolds number for plane channel flow and 1/5 in the Blasius boundary-layer case, and some nonlinear features of channel flows were also investigated. Since then separate developments have taken place in the use of reduced NS, parabolized stability, and other equations, in a similar spirit. The plan of the present work is to concentrate on the nonlinear boundary-layer case and follow through the suggestions from Smith *et al.* [1] (see also [8], [9], [11] and [12]) on the modified use of interactive-boundary-layer ideas in the unsteady flow at large Reynolds numbers, ideas which have proved successful in the field of steady aerodynamic computations for example (Davis and Werle [13]). We note in addition that there are a number of interesting computations on unsteady interacting boundary layers with zero normal pressure gradient, in two-dimensional flow (Smith [14], Duck [15], Henkes and Veldman [16], Peridier *et al.* [17]) and three-dimensional flow (Smith [18]), but the limitations on these with regard to sublayer bursting and singularities for instance are shown theoretically in references [8, 9, 11]; removal of the limitations corresponds to the inclusion of normal-pressure-gradient effects (see last references), pointing to the suggestions in Smith *et al.* [1].

The Composite or unified treatment (see Section 2) is intended to solve accurately a reduced set of equations appropriate for the large-Reynolds-number flows in question, incorporating especially the viscous-inviscid interactions of Tollmien-Schlichting (TS) waves for instance as well as inviscid inflexional instabilities, and including significant normal-pressure-gradient contributions. The Composite approach is then used as the basis for the alternative NS and Euler approaches (see Sections 3, 4), in which the extra/different terms required in the equations are simply added in passively during the iterative routine. A major aim here is to compare the results from the various approaches, at large Reynolds numbers (see below), and compare their work rates, features which are considered in Section 5. As a start, therefore, streamwise (x) periodicity, two-dimensionality and incompressibility are assumed throughout, for unsteady boundary-layer flow past a flat surface ($y = 0$) with freestream unsteadiness acting. Extensions are mentioned later in Section 5. Here nondimensionalized velocity components u, v in Cartesian coordinates x, y, time t and pressure p are taken, based on the characteristic free-stream speed and on the typical boundary-layer thickness, as is the local

Reynolds number R, while the associated global Reynolds number based on the airfoil chord is $Re(= R^2)$. Since our current interest is mostly in local properties, especially transition, the computations are focussed normally within and just outside the boundary layer. This is designed to capture much of both gradual and by-pass transitions, the former having the slightly longer (TS) nonlinear length scales (theory, Smith [8] for example) at first, whereas the latter have length scales comparable with the boundary-layer thickness and smaller (see the Euler stage and scale cascades in references [8, 10], Bowles and Smith [19]). Bursting and sublayer eruption can also be handled in principle by the Euler- or normal-pressure-gradient contributions present, provided viscous effects act also (otherwise bursting is absent): again see the theory in reference [8]. Similar comments apply to steady separating flow and stall, where again there is a need for local Euler-like regions to be accommodated in the numerical procedures: references [8, 9, 11]. Not all of the issues raised above can be settled here, but, on one issue, it is found that the Composite, NS and Euler approaches are in good agreement at global Reynolds numbers Re of about 10^7–10^8, corresponding to local Reynolds numbers R of 6000–12000, for the time ranges and particular disturbances considered.

2. The unsteady composite scheme

The governing equations in the Composite approach are the unsteady interacting boundary-layer (IBL) equations but supplemented by normal pressure-gradient effects:

$$\frac{\partial u}{\partial x} + \frac{\partial v}{\partial y} = 0, \tag{2.1a}$$

$$\frac{\partial u}{\partial t} + u\frac{\partial u}{\partial x} + v\frac{\partial u}{\partial y} = -\frac{\partial p}{\partial x} + R^{-1}\frac{\partial^2 u}{\partial y^2}, \tag{2.1b}$$

$$\frac{\partial v}{\partial t} + u\frac{\partial v}{\partial x} + \Gamma v\frac{\partial v}{\partial y} = -\frac{\partial p}{\partial y}. \tag{2.1c}$$

First we consider Γ *zero*, as suggested in [1]. Among the main reasons for focussing initially on the system (2.1a–c) are these: it captures the linear and nonlinear behavior of TS waves (lower-branch, upper-branch, and in-between) and of inflexional waves to a large extent; it appears to reflect also the nonlinear break-up dynamics involved in the unsteady IBL equations alone ([8, 9, 11]); it allows much of the nonlinear-TS and Euler stages ([8, 10]) to be incorporated together; and yet it is simpler than the NS system, as well as pointing to alternative NS and Euler treatments, described in the next sections. The boundary conditions on the system include

$$u \to u_e(t), \quad \frac{\partial p}{\partial x} \to Q(t) \text{ as } y \to \infty, \tag{2.1d}$$

$$u = v = 0 \text{ at } y = 0, \tag{2.1e}$$

$$\text{upstream -}x\text{ and downstream -}x\text{ constraints,} \tag{2.1f}$$

together with the initial conditions at time zero. In (2.1d), $u_e(t)$ is the given unsteady freestream velocity, independent of x, with streamwise pressure gradient $Q(t)$ such that $u_e'(t) = -Q(t)$, and (2.1e) is the no-slip constraint. More details on the above conditions are given in the following, while Section 1 includes mention of the interactive nature of (2.1d).

Computational solutions of (2.1a–c) were obtained by a spectral method, as a starting point, with spatial periodicity in x of wavelength $2\pi/\alpha$ assumed. Thus Fourier series of the form

$$(u,\psi) = (u_o,\psi_o) + \sum_1^\infty [(u_n,\psi_n)E^n + (\hat{u}_n,\hat{\psi}_n)E^{-n}], \tag{2.2a}$$

$$p = xQ(t) + \sum_0^\infty [p_n E^n + \hat{p}_n E^{-n}] \tag{2.2b}$$

hold, where ψ is the stream function and $\hat{}$ stands for the complex conjugate. Also, the known pressure-gradient function $Q(t)$, and the unknowns $(u_o,\psi_o)(y,t)$, are real, the unknowns $(u_n,\psi_n,p_n)(y,t)$ for $n \neq 1$ are complex in general, and

$$E \equiv \exp(i\alpha x). \tag{2.3}$$

So the Composite equations (2.1a–c) yield formally, after some rearrangement, the component equations

$$u_n = \partial\psi_n/\partial y [n \geqslant 0], \tag{2.4a}$$

$$\frac{\partial u_n}{\partial t} + i(n\alpha)\left[u_o u_n - \psi_n \frac{\partial u_o}{\partial y} + p_n\right] - \frac{1}{R}\frac{\partial^2 u_n}{\partial y^2} = \mathcal{L}_n \quad \text{for} \quad n \geqslant 1, \tag{2.4b}$$

$$\frac{\partial u_o}{\partial t} + Q(t) - \frac{1}{R}\frac{\partial^2 u_o}{\partial y^2} = \mathcal{L}_o, \tag{2.4c}$$

$$-i(n\alpha)\frac{\partial \psi_n}{\partial t} + (n\alpha)^2 u_o \psi_n + \frac{\partial p_n}{\partial y} = \mathcal{M}_n \quad \text{for} \quad n \geqslant 1, \tag{2.4d}$$

$$2\frac{\partial p_o}{\partial y} = \mathcal{M}_o. \tag{2.4e}$$

Here the contributions on the right-hand sides are given by

$$\begin{aligned} i\alpha^{-1}\mathcal{L}_n = & \sum_{m=1}^{n-1}\left[(n-m)u_m u_{n-m} - m\psi_m \frac{\partial u_{n-m}}{\partial y}\right] \\ & + \sum_{m=1}^{\infty}\left[(m+n)\hat{u}_m u_{m+n} + m\hat{\psi}_m \frac{\partial u_{m+n}}{\partial y}\right] \\ & + \sum_{m=n+1}^{\infty}\left[(m-n)u_m \hat{u}_{m-n} - m\psi_m \frac{\partial \hat{u}_{m-n}}{\partial y}\right], \end{aligned} \tag{2.5a}$$

$$i\alpha^{-1}\mathcal{L}_o = \sum_{m=1}^{\infty} m\left(\hat{\psi}_m \frac{\partial u_m}{\partial y} - \psi_m \frac{\partial \hat{u}_m}{\partial y}\right), \tag{2.5b}$$

$$\begin{aligned} -\alpha^{-2}\mathcal{M}_n = & \sum_{m=1}^{n-1}(n-m)^2 u_m \psi_{n-m} + \sum_{m=n+1}^{\infty}(m-n)^2 u_m \hat{\psi}_{m-n} \\ & + \sum_{m=1}^{\infty}(m+n)^2 \hat{u}_m \psi_{m+n}, \end{aligned} \tag{2.5c}$$

$$-\alpha^{-2}\mathcal{M}_o = \sum_{m=1}^{\infty} m^2(u_m\hat{\psi}_m + \hat{u}_m\psi_m), \tag{2.5d}$$

containing only nonlinear terms.

A fairly straightforward finite-difference implicit scheme is adopted for (2.4)–(2.5). More sophisticated differencing, iteration or other numerical devices could be used at this stage but our prime concern is more with the value and accuracy of the Composite-equation approach as compared with the others described in the subsequent sections. For (2.4a, b, d) we discretized the equations in the second-order accurate (in space and time) form

$$\frac{1}{2}(\tilde{u}_{nj} + \tilde{u}_{nj-1}) = (\tilde{\psi}_{nj} - \tilde{\psi}_{nj-1})/\Delta y [2 \leqslant j \leqslant J], \tag{2.6a}$$

$$\frac{2}{\Delta t}[\tilde{u}_{nj} - u_{nj}^{(o)}] + in\alpha[\tilde{u}_{oj}\tilde{u}_{nj} - \tilde{\psi}_{nj}(\tilde{u}_{oj+1} - \tilde{u}_{oj-1})/(2\Delta y) + \tilde{p}_n] - R^{-1}[\tilde{u}_{nj+1} - 2\tilde{u}_{nj} + \tilde{u}_{nj-1}]/(\Delta y)^2 = \tilde{\mathcal{L}}_{nj}[2 \leqslant j \leqslant J-1], \tag{2.6b}$$

$$-\frac{in\alpha}{\Delta t}[\tilde{\psi}_{nj} + \tilde{\psi}_{nj-1} - \psi_{nj}^{(o)} - \psi_{nj-1}^{(o)}] + \frac{n^2\alpha^2}{4}(\tilde{u}_{oj} + \tilde{u}_{oj-1})(\tilde{\psi}_{nj} + \tilde{\psi}_{nj-1}) + (\tilde{p}_{nj} - \tilde{p}_{nj-1})/\Delta y = \tilde{\mathcal{M}}_{nj-1/2}[2 \leqslant j \leqslant J], \tag{2.6c}$$

and similarly for (2.4c, e). Here (o) and (c) denote the values at the (known) previous and (unknown) current time levels t, $t + \Delta t$ respectively, $\tilde{}$ the (unknown) average of these values, e.g. $\tilde{u} = (u^{(c)} + u^{(o)})/2$, $J - 1$ is the number of y-steps, with step length Δy, while $(J-1)\Delta y = y_2$ fixes the outer boundary, and the subscript j stands for evaluation at $(j-1)\Delta y$ and so on. Analogous differencing is performed on the contributions in (2.5), to produce the terms on the right-hand sides in (2.6b, c), where any averaging necessary is done as locally as possible, i.e. as in the term involving $(n\alpha)^2$ in (2.6c), and tilde variables are used again to preserve the order $(\Delta t)^2$ accuracy. With the solution for $(\psi, u, p)_{nj}^{(o)}$ for all n known at time t, a first guess is made for the corresponding unknown tilde values. Then, for each n, (2.6a–c) $(n \geqslant 1)$ or the counterparts for n zero (see below) are solved together with the constraints

$$\tilde{u}_{n1} = \tilde{\psi}_{n1} = 0, \tag{2.6d}$$

$$\tilde{u}_{nJ} = 0, \tag{2.6e}$$

to give updated values of $(\tilde{\psi}, \tilde{u}, \tilde{p})_{nj}$, with the other components $\tilde{\psi}_m$, $m \neq n$, etc., being kept at their latest stored values. This is done in turn for all the n $(n \geqslant 0)$ values and is then repeated, until all the successive iterates are sufficiently close in value. So $\psi^{(c)}$ follows from $\psi^{(c)} = 2\tilde{\psi} - \tilde{\psi}^{(o)}$, etc., and the procedure can move on to the next time step. In solving (2.6a–e) for $(\tilde{\psi}, \tilde{u}, \tilde{p})_{nj}$ $(n \geqslant 1)$ the scheme uses inversion of a 3×3 block double-diagonal matrix. In deriving the mean-flow quantities ψ_o, u_o, Q, p_o during each iteration, on the other hand, a slightly different approach is taken, since the counterpart of (2.6b) for $n = 0$ has $\tilde{\psi}_{oj}$ absent on the left-hand side. Thus (2.6b), with $\tilde{Q}$ included, produces a tridiagonal system for the $\tilde{u}_{oj}$ values subject to

$$\tilde{u}_{oj} = \begin{cases} 0 & \text{at } j = 1, \quad (2.7a) \\ 1 - \int_o^{\tilde{t}} Q(t)\mathrm{d}t & \text{at } j = J, \quad (2.7b) \end{cases}$$

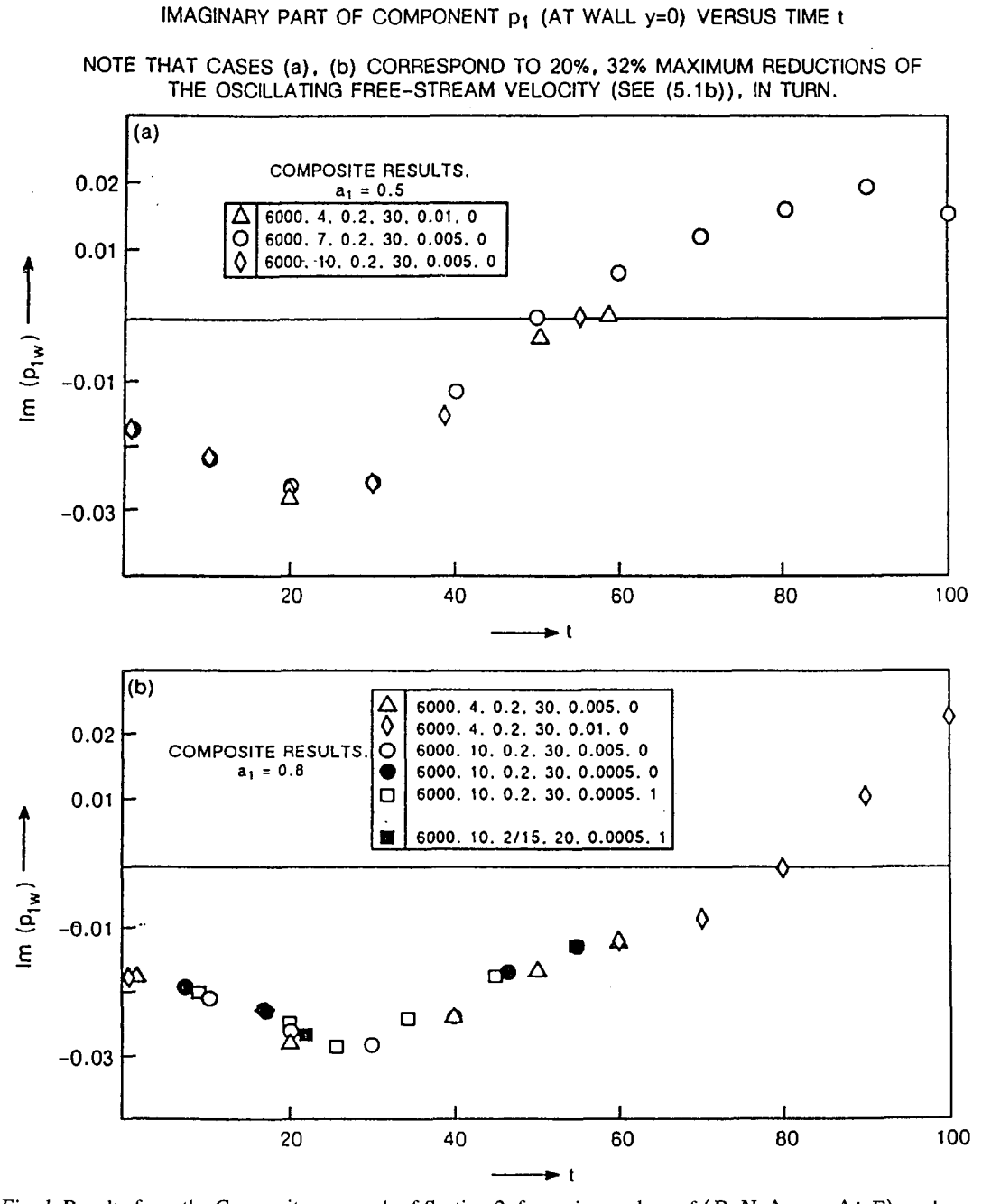

Fig. 1. Results from the Composite approach of Section 2, for various values of $(R, N, \Delta y, y_2, \Delta t, \Gamma)$ as shown above, with $\alpha = 0.2, \omega_1 = 5$ throughout.

which determines the $\tilde{u}_{oj}$ updates; here $\tilde{t} \equiv t + \Delta t/2$ and the initial value $u_e(0) = 1$ without loss of generality. Following that, the $\tilde{\psi}_{oj}$ updates can be obtained marching (2.6a) upwards in j, given the surface value $\tilde{\psi}_{o1} = 0$; while the remaining equation (2.6c) fixes the mean normal

MEAN-FLOW VELOCITY COMPONENT u_0, NEAR WALL (y = Δy). HERE a_1 = 0.8, PARAMETERS (6000, 10, 0.2, 30, 0.005). THE FREE-STREAM FORCING PERIOD $2\pi/\omega_1$ IS ALSO INDICATED, FOR COMPARISON

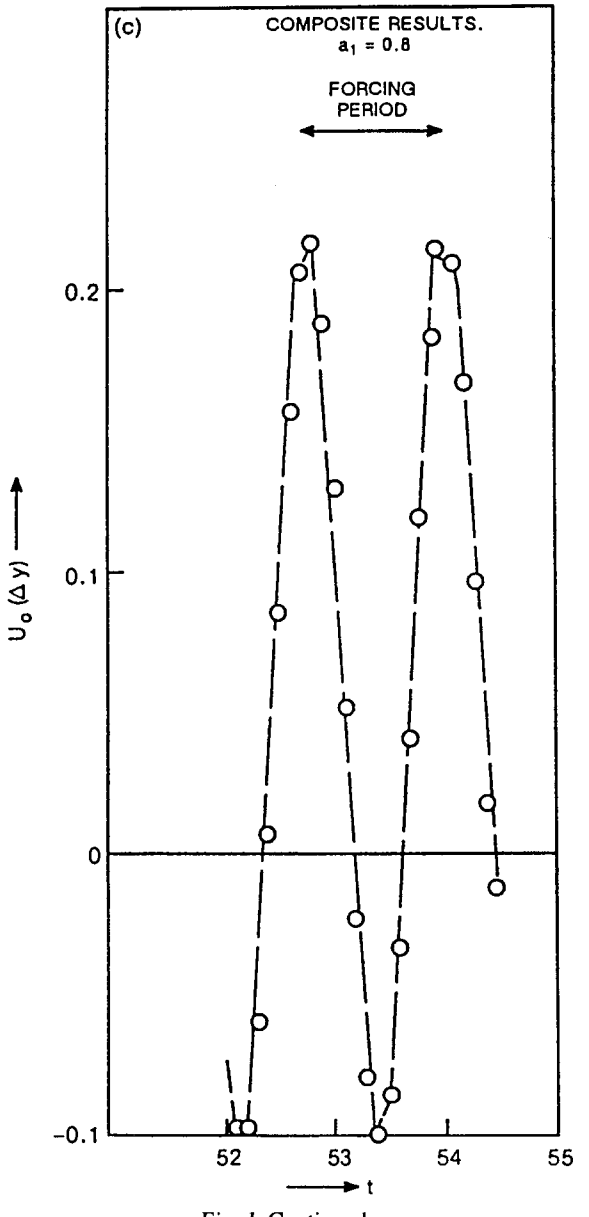

Fig. 1. Continued.

pressure gradient, or, on integration downwards, the mean surface pressure $\tilde{p}_{o1}$ effectively, taking $\tilde{p}_{oJ}$ as given from (2.1d), (2.2b); (2.6c) is otherwise redundant for n = zero.

Results for representative quantities are presented subsequently in Figs. 1 and 4 and are discussed in Section 5 below. Typical values taken in the computations were $[N, \Delta y, \Delta t, y_2, q] = [7, 0.2, 0.002, 30, 10^{-6}]$ where N is the number of Fourier modes included and q is the iterative

tolerance per timestep. Checks on the influences of the various grid and iteration parameters are also described in Section 5.

The Composite scheme has also been used in this research with Γ *unity*, in (2.1c). The extra term $v\,\partial v/\partial y$ is incorporated in the computational routine by using the 'rolling in' approach, during the iterations, as in the work of the next two sections (cf. ref. [20]). Typical results are described in Section 5.

3. The unsteady NS scheme

Here the new approach to deriving full NS solutions for the unsteady nonlinear boundary-layer responses is described, based on the Composite method of Section 2 (with zero Γ) and analogous to the channel-flow approach in [1].

The NS equations, for comparison, are

$$\frac{\partial u}{\partial x}+\frac{\partial v}{\partial y}=0, \tag{3.1a}$$

$$\frac{\partial u}{\partial t}+u\frac{\partial u}{\partial x}+v\frac{\partial u}{\partial y}=-\frac{\partial p}{\partial x}+R^{-1}\left(\frac{\partial^2 u}{\partial y^2}+\frac{\partial^2 u}{\partial x^2}\right), \tag{3.1b}$$

$$\frac{\partial v}{\partial t}+u\frac{\partial v}{\partial x}+v\frac{\partial v}{\partial y}=-\frac{\partial p}{\partial y}+R^{-1}\left(\frac{\partial^2 v}{\partial y^2}+\frac{\partial^2 v}{\partial x^2}\right). \tag{3.1c}$$

The extra contributions from the terms $R^{-1}\partial^2 u/\partial x^2$ in (3.1b) and $v\,\partial v/\partial y$, $R^{-1}(\partial v^2/\partial y^2+\partial^2 v/\partial x^2)$ in (3.1c), which are omitted in (2.1b,c), are now added to the right-hand sides $\mathcal{L}_n$, $\mathcal{M}_n$ [in (2.4b–e)] following the decomposition (2.2a, b). This is done in a passive fashion, given that in many situations of interest these extra contributions are only subsidiary parts of the physics controlling the nonlinear unsteady flows at large R, according to theory (see Refs.). This tends to be borne out by, first, the resulting numerical closeness of the present solutions and those from Section 2 and, second, the lack of significant extra work required to change from (2.1a–c) to (3.1a–c), as discussed later in Section 5. The additions to $i\alpha^{-1}\mathcal{L}_n$ in (2.5a, b) required here are therefore

$$-\frac{i(n\alpha)^2}{\alpha R}u_n, \tag{3.2a}$$

for $n \geqslant 0$, and the additions to $-\alpha^{-2}\mathcal{M}_n$ in (2.5c, d) are

$$\frac{i(n\alpha)}{\alpha^2 R}\left[\frac{\partial u_n}{\partial y}-(n\alpha)^2\psi_n\right]-\sum_{m=1}^{n}m(n-m)\psi_m u_{n-m}+\sum_{m=n+1}^{\infty}m(m-n)\psi_m\hat{u}_{m-n}$$
$$+\sum_{m=1}^{\infty}m(m+n)\hat{\psi}_m u_{m+n}, \tag{3.2b}$$

for $n \geqslant 1$. The NS contributions (3.2a, b), discretized in similar fashion to Section 2, are added to (2.5a, b), (2.5c, d) respectively [i.e. to (2.6b, c)] at each iteration per time level. In all other respects the discretization and routines described in Section 2 are unaltered throughout.

The outcome of the present NS approach computations is considered in Section 5, together with relevant comparisons; see Figs. 2 and 4. The grid parameters used are by and large the same as for the Composite approach of Section 2.

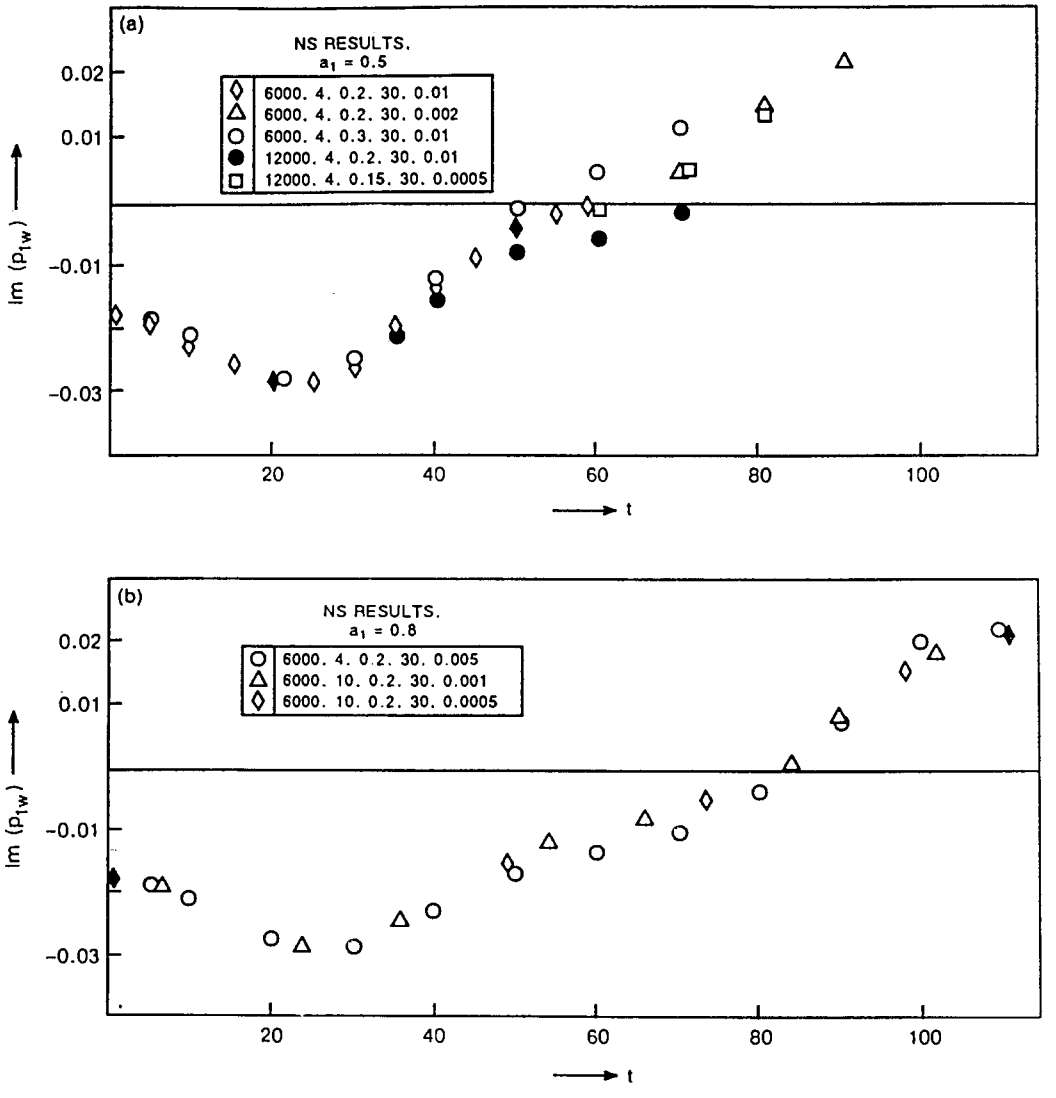

Fig. 2. Results from the NS approach of Section 3, with $(R, N, \Delta y, y_2, \Delta t)$ as shown and $\alpha = 0.2, \omega_1 = 5$.

4. The unsteady Euler scheme

The unsteady nonlinear Euler-flow solutions described below are obtained in similar vein to Section 3. Again for comparison, the governing equations here are

$$\frac{\partial u}{\partial x} + \frac{\partial v}{\partial y} = 0, \tag{4.1a}$$

$$\frac{\partial u}{\partial t} + u\frac{\partial u}{\partial x} + v\frac{\partial u}{\partial y} = -\frac{\partial p}{\partial x}, \tag{4.1b}$$

$$\frac{\partial v}{\partial t} + u\frac{\partial v}{\partial x} + v\frac{\partial v}{\partial y} = -\frac{\partial p}{\partial y}, \tag{4.1c}$$

MEAN-FLOW VELOCITY COMPONENT u_0, NEAR WALL ($y = \Delta y$), AT RELATIVELY LATE TIMES t. HERE $a_1 = 0.8$, PARAMETERS (6000, 10, 0.2, 30, 0.0005). THE FREE-STREAM FORCING PERIOD $2\pi/\omega_1$ IS ALSO INDICATED, FOR COMPARISON

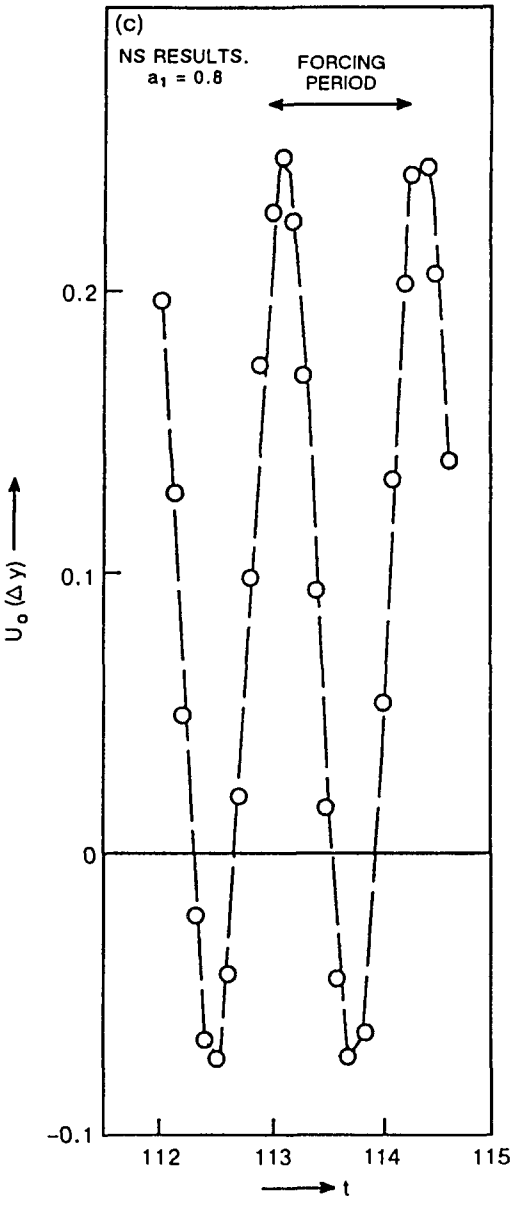

Fig. 2. Continued.

So all the viscous terms, involving R^{-1}, in (2.4a)–(2.5d) supplemented by (3.2a, b), are omitted in the Euler computations. Together with this, the number of surface conditions must be reduced of course, with only $\tilde{\psi}_{n1} = 0$ rather than (2.6d), but, to compensate, the streamwise momentum equation (2.6b) can now be applied at one extra y-point. Again, we choose to keep the outer condition (2.6e) here, although the results obtained with other constraints, namely

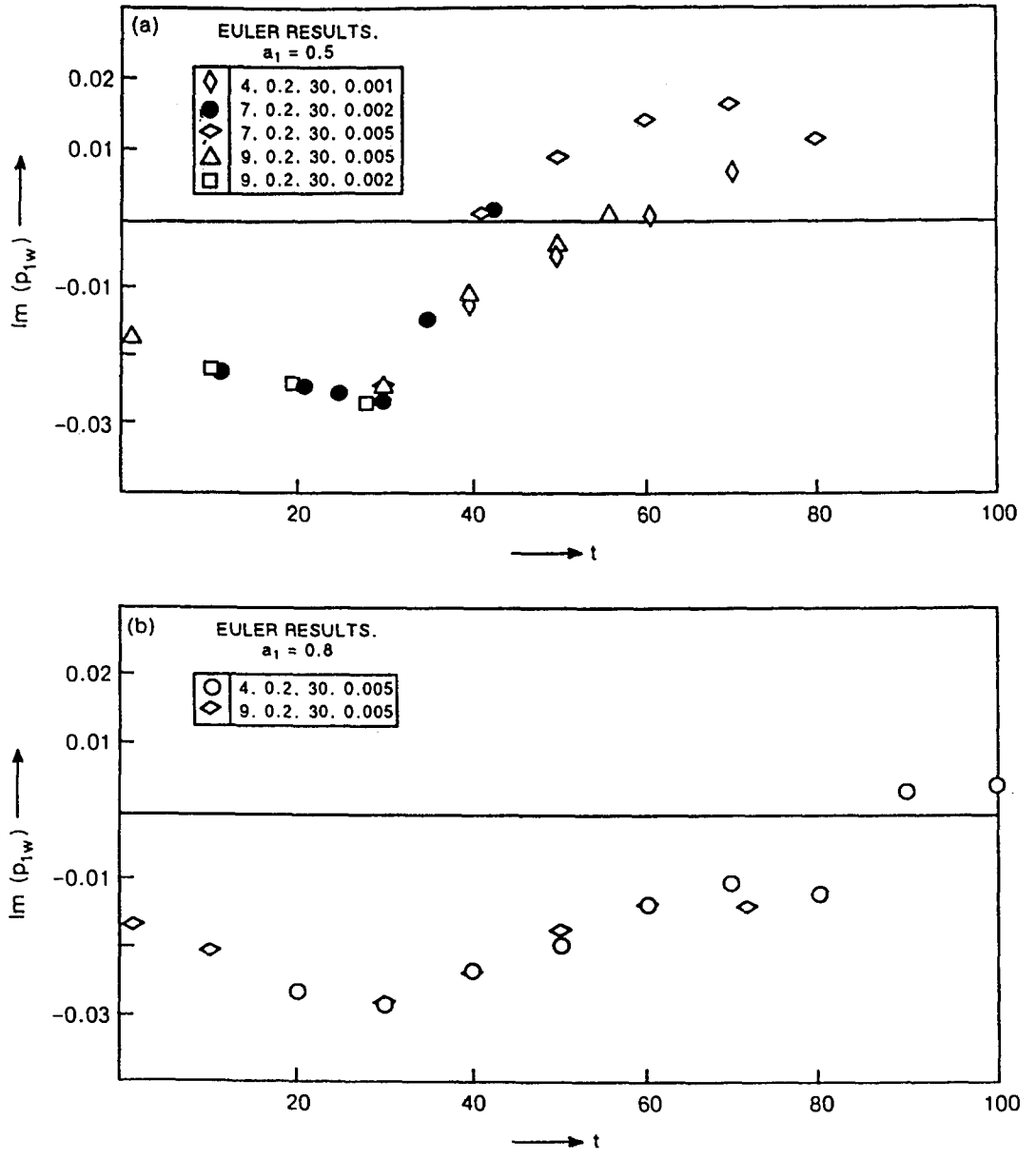

Fig. 3. Results from the Euler approach of Section 4, with $(N, \Delta y, y_2, \Delta t)$ as shown and $\alpha = 0.2, \omega_1 = 5$.

$\tilde{\psi}_{nJ}$ or $\tilde{p}_{nJ}$ set to zero, proved to be virtually identical with the present ones. An alteration is also necessary for the mean-flow $(n = 0)$ terms, where we integrate

$$\frac{2}{\Delta t}[\tilde{u}_{oj} - u_{oj}^{(o)}] = \tilde{\mathcal{L}}_{oj} - Q\left(t + \frac{\Delta t}{2}\right) \tag{4.2}$$

directly for all the $\tilde{u}_{oj}$ values, $j = 1$ to J, after which the $\tilde{\psi}_{oJ}$ updates stem from (2.6a), given $\tilde{\psi}_{o1} =$ zero.

The rest of the discretization and iteration routines are maintained exactly as in Section 2, supplemented by (3.2a, b) with zero R^{-1}. The grid parameters used are again broadly the

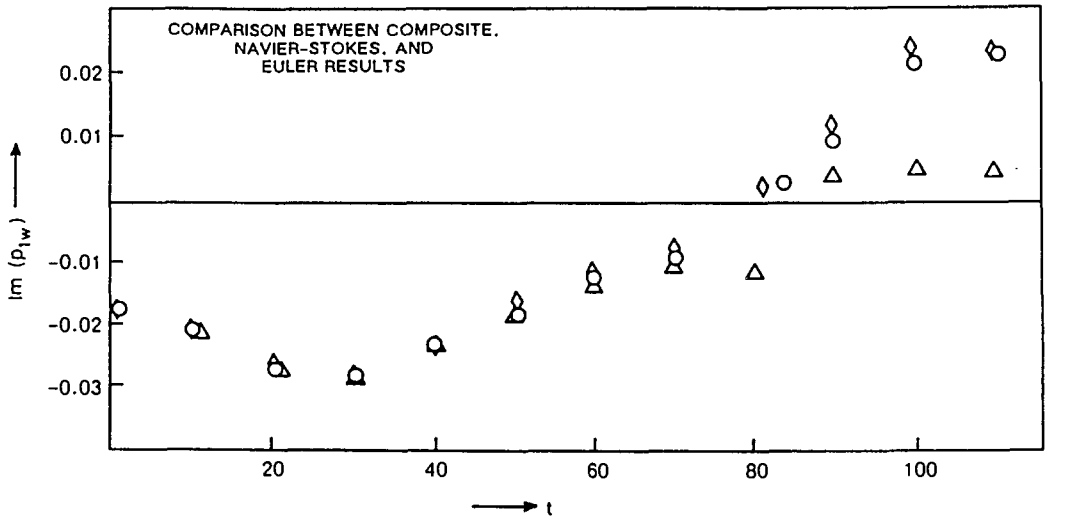

Fig. 4. Comparisons between the Composite, Navier–Stokes and Euler results (shown as ◊, ○, △, respectively), computed on typical grids, with $\alpha = 0.2$, $\omega_1 = 5$, $a_1 = 0.8$. Reynolds number $R = 6000$ in the first two cases.

same as for Section 2 except that slightly smaller time steps Δt tend to be necessary. Results for the Euler equations (4.1a–c) are presented in the next section, along with comparisons with those of Sections 2 and 3; see Figs. 3 and 4 below.

5. Results, comparisons and discussion

Results from the Composite approach of section 2 are shown in Fig. 1, while Figs. 2 and 3 show results from the Navier–Stokes (Section 3) and Euler (Section 4) schemes in turn. In all cases the initial values taken are

$$\left.\begin{aligned} &u_o = 1 - e^{-y}, u_1 = iy[\exp(-y^2) - 2\exp(-2y^2)], \\ &u_n = 0 \text{ for } n \geqslant 2, \quad p_n = 0 \text{ for } n \geqslant 0, \end{aligned}\right\} \tag{5.1a}$$

at $t = 0$, with the ψ_n values following from (2.4a), and the edge velocity and streamwise pressure gradient for $t \geqslant 0$ are given by

$$u_e(t) = 1 + a_1\omega_1^{-1}[\cos(\omega_1 t) - 1], \quad Q(t) = a_1 \sin(\omega_1 t). \tag{5.1b}$$

The computations were run for the order of 10^4–10^5 time steps, requiring about 5 iterative sweeps per time step. The Figs. 1–3 also include some grid-effect studies in terms of the y-grid, the t-step and the number of spectral modes, as well as the influence of the local Reynolds number R, and the influence of altering Γ in (2.1c) from zero to unity. The three approaches of Sections 2–4 took virtually the same computer time, for a given grid and Reynolds number. Again, tests on the accuracy to which the approaches satisfy the governing equations [(2.1), (3.1) or (4.1)] were performed as in [1] with broadly similar results: satisfaction was achieved typically to well within 1% of the maximum term in the equations, throughout the present computations.

In the results of Figs. 1–3 we observe the spatial mean-flow ($n = 0$) quantities responding at approximately the forcing frequency ω_1 imposed in (5.1b), whereas the much slower evolution

of the spatial first-harmonic ($n = 1$) property as plotted is of more concern here. This is in general agreement with limiting analyses of (2.1), (3.1) or (4.1), e.g. for small times t.

Comparisons between the results from the three methods of Section 2–4 are presented in Fig. 4. These are close overall and tend to encourage the use of the present approaches at such higher Reynolds numbers. Indeed, the main cause of any inaccuracy in the computations so far would seem to be due much more to grid resolution, including the streamwise spectral truncation, than to the differences in three sets of governing equations addressed in Sections 2–4. That conclusion may be modified at later times, however, when vortex shedding from the viscous sublayer near the surface occurs in the Composite and Navier–Stokes approaches of Sections 2 and 3 but is missed by the inviscid Euler approach of Section 4. There is a little evidence of this in the comparisons above, and we note also that mean-flow reversal does take place near the surface, at increased forcing amplitude, accompanied by significant increases in the amplitudes of the higher spectral modes. (A similar modification may apply for increased wavenumbers α. Preliminary results have been obtained for α values up to 5, with the current schemes, and also for surface conditions corresponding to unsteady injection and suction, but these have not been investigated sufficiently thoroughly yet with respect to grid-resolution effects.)

A number of other related points should be mentioned here. First, this work on the non-linear unsteady boundary layer has assumed spatial periodicity, incompressibility and two-dimensionality, as a convenient starting point. Clearly for practical reasons the extensions to spatially growing motion, to compressible flows, and to the three-dimensional setting are called for , and ideas similar to those in Sections 2–4 do apply in those more realistic contexts; see also [19] and below. Second, the procedure for the Euler-equation solver in particular, in Section 4, may not be especially efficient, although again there appear to be few other methods reported in the literature, for the present flow conditions. Third, comparisons with other computational methods and results would be desirable at the higher Reynolds numbers of interest for these flows, given that most previous computational studies in contrast tend to address relatively low Reynolds numbers. In that regard, the comparisons in [1] for the linearized version in the boundary-layer case, at relatively low Reynolds numbers (see in Section 1), also provide much encouragement.

It is felt that the way is now open, in principle, for many useful applications in dynamic stall and boundary-layer transition. Some substantial questions remain to be answered; for example, on the need for extremely sensitive grid resolution (e.g. with adaptive gridding) during vortex eruption and subsequent dynamic stall; on the merits of two-dimensional or quasi-planar methods during fully fledged transition as opposed to three-dimensional methods (theory in [8, 9, 11] suggests quasi-planar processes might dominate certain aspects of transition in its later stages, including vortex eruption); and on the implementation of the three-dimensional versions necessary, quite possibly based on the computational studies of steady and unsteady interactive three-dimensional boundary layers in [18, 21]. This should allow firmer comparisons to be made with experiments on full transition and on by-pass transition, e.g. see those in [22]. Throughout, the benefits of a substantial theoretical input seem fairly clear in numerical terms. (In particular, for the present contexts, we note the agreement found recently between the numerical work of [17] and the theory in [11] concerning unsteady interacting boundary layers and their role in dynamic stall and possibly in intermittency during transition.)

Acknowledgement

Many thanks are due to Dr M. Barnett and Prof. A. P. Rothmayer, for discussions on this work and their related studies, to them and to Dr J. E. Carter, Dr D. J. Doorly, Dr J. M. Verdon and Prof. J. D. A. Walker, for many helpful comments, to the United Technologies Independent Research Program for support, and to SERC, EPSRC and ULCC, U.K., for computer resources.

References

1. F. T. Smith, D. T. Papageorgiou and J. W. Elliott, *J. Fluid Mech.* 146 (1984) 313–330.
2. E. R. Van Driest and C. B. Blumer, *A.I.A.A. J.* 1 (6), (1963) 303-314.
3. J. Dunham, *Predictions of Boundary-Layer Transition on Turbomachinery blades.*
4. W. B. Roberts, A.I.A.A. paper No. 79-0285 (1979) presented at New Orleans mtg.
5. B. J. Abu-Ghannam and R. Shaw, *J. Mech. Eng. Sci.*, 22, (5), (1980) 213–228.
6. R. Narasimha, *Prgr. Aerospace Sci.*, 22 (1985) 29–80.
7. J. L. Van Ingen, T. H. Delft, Dept. Aerospace Sciences, Netherlands, Rept. VTH71 (1956).
8. F. T. Smith, *Invited Lecture ICTAM Conf. Grenoble* (1988) pub. Springer-Verlag (1989); *A.I.A.A. Jnl.*, 31 (1993) 2220–2226.
9. J. M. Hoyle, F. T. Smith and J. D. A. Walker, *Comput. Phys. Commns.* 65 (1991) 151–157.
10. F. T. Smith, D. J. Doorly and A. P. Rothmayer, *Proc. Roy. Soc.*, A 428 (1990) 255–281: extension of UTRC Rept. 87–43. Un. Tech. Res. Ctr. Hartford (Conn) (1987).
11. F. T. Smith, *Mathematika*, 35 (1988) 256–273.
12. S. G. Rubin and J. C. Tannehill, *Ann. Rev. Fluid Mechs.*, 24 (1992) 117–144.
13. R. T. Davis and M. J. Werle, in Proc. Conf. Num. and Phys. *Aspects of Aerodyn. Flows* (ed. T. Cebeci) Long Beach, Calif., pub. Springer-Verlag, New York (1982).
14. F. T. Smith, A.I.A.A. paper no. 84-1582 (1984) presented at A.I.A.A. mtg. Snowmass, Colorado, and (1985, 1986) UTRC Rept. 85–36. Un. Tech. Res. Ctr. Hartford (Conn) *J. Fluid Mech.*, 169, 353–377.
15. P. W. Duck, *J. Fluid Mech.*, 160 (1985) 465–498.
16. R. A. W. M. Henkes and A. E. P. Veldman, in *Boundary-Layer Separation* (eds. F. T. Smith and S. N. Brown), Springer-Verlag, (1987); and *J. Fluid Mech.*, 179 (1987) 513–529.
17. V. J. Peridier, F. T. Smith and J. D. A. Walker, *J. Fluid Mech.*, 232 (1991) 133–165.
18. F. T. Smith, presented at R. T. Davis Mem. Symp. (1987) Cincinnati, Ohio, June 1987; Computers & Fluids 20 (1991) 243–268.
19. R. I. Bowles and F. T. Smith, UTRC Rept. 89–26 (1989); Smith UTRC Rept. 87–52 (1987) (*J. Fluid Mech.*, 198, 127–153); *J. Eng. Maths.*, 27 (1993) 309–342.
20. M. Israeli and A. Lin, *Computers & Fluids*, 13 (1985) 397–409.
21. D. E. Edwards and F. T. Smith, UTRC Report 88–35 (1988) (and F. T. Smith, UTRC Rept. (1983) 83–46 Un. Tech. Res. Ctr. Hartford (Conn)).
22. F. T. Smith and R. I. Bowles, *Proc. Roy. Soc.*, A 439 (1992) 163–175.